Using Z_{DR} Columns in Forecaster Conceptual Models and Warning Decision-Making

CHARLES M. KUSTER,[a,b,c] TERRY J. SCHUUR,[a,b,c] T. TODD LINDLEY,[d] AND JEFFREY C. SNYDER[b]

[a] *Cooperative Institute for Mesoscale Meteorological Studies, Norman, Oklahoma*
[b] *NOAA/OAR National Severe Storms Laboratory, Norman, Oklahoma*
[c] *University of Oklahoma, Norman, Oklahoma*
[d] *NOAA/National Weather Service, Norman, Oklahoma*

(Manuscript received 26 May 2020, in final form 23 September 2020)

ABSTRACT: Research has shown that dual-polarization (dual-pol) data currently available to National Weather Service forecasters could provide important information about changes in a storm's structure and intensity. Despite these new data being used gradually by forecasters more over time, they are still not used extensively to inform warning decisions because it is unclear how to apply dual-pol radar data to specific warning decisions. To address this knowledge gap, rapid-update (i.e., volumetric update time of 2.3 min or less) radar data of 45 storms in Oklahoma are used to examine one dual-pol signature, known as the differential reflectivity (Z_{DR}) column, to relate this signature to warning decisions. Base data (i.e., Z_{DR}, reflectivity, velocity) are used to relate Z_{DR} columns to storm intensity, radar signatures such as upper-level reflectivity cores, and scientific conceptual models used by forecasters during the warning decision process. Analysis shows that 1) differences exist between the Z_{DR} columns of severe and nonsevere storms, 2) Z_{DR} columns develop and evolve prior to upper-level reflectivity cores, 3) rapid-update radar data provide a more complete picture of Z_{DR} column evolution than traditional-update radar data (i.e., volumetric update time of about 5 min), and 4) Z_{DR} columns provide a clearer and earlier indication of changes in updraft strength compared to reflectivity signatures. These findings suggest that Z_{DR} columns can be used to inform warning decisions, increase warning confidence, and potentially increase warning lead time especially when they are integrated into existing conceptual models about a storm's updraft and intensity.

KEYWORDS: Atmosphere; Mesoscale processes; Radars/Radar observations; Operational forecasting; Short-range prediction

1. Introduction

Weather radar provides crucial remotely sensed information about the intensity and structure of convective storms that National Weather Service (NWS) forecasters can apply to scientific conceptual models of storm processes in order to anticipate hazardous weather phenomenon during the warning decision process (e.g., Andra et al. 2002). As radar technology advances, more information becomes available to NWS forecasters and their understanding of how conceptual models can be applied to the severe weather warning decision process improves. Such an advancement recently occurred with the dual-polarization (dual-pol) upgrade of the Weather Surveillance Radar-1988 Doppler (WSR-88D) radar network (NOAA 2013). This upgrade made available several additional radar variables that led to the identification of signatures that aid in diagnosing changes in a storm's organization and intensity (e.g., Kumjian and Ryzhkov 2008; Romine et al. 2008; Crowe et al. 2012; Kumjian 2013). One of these dual-pol variables is differential reflectivity (Z_{DR}), which is the difference between horizontal reflectivity and vertical reflectivity (when reflectivity is provided in units of dBZ). In general, Z_{DR} is positive for hydrometeors that are aligned primarily with the largest axis in the horizontal, as is the case for rain drops and wet ice, which become more oblate as drop size increases (e.g., Herzegh and Jameson 1992). One potentially useful dual-pol signature is a vertically continuous column of positive Z_{DR} extending above the environmental melting layer known as the Z_{DR} column (e.g., Illingworth et al. 1987; Tuttle et al. 1989; Kumjian et al. 2014). Consideration of Z_{DR} columns may be important for NWS forecasters because they can provide information about the location and intensity of a storm's updraft (e.g., Ryzhkov et al. 1994; Kumjian et al. 2014; Snyder et al. 2015).

Despite the potentially beneficial information Z_{DR} columns and other dual-pol signatures can provide, dual-pol data are not extensively used by NWS forecasters in real-time to make warning decisions. Its use is slowly increasing but may still be limited partially due to the sparsity of research that explicitly links dual-pol signatures to existing scientific conceptual models and the warning decision process as well as situations in which dual-pol data can specifically add beneficial information to what is already provided by single-polarization data. During the stressful complexities of severe convective warning operations, forecasters tend to revert to proven conceptual understandings of severe storm structure, such as but not limited to, reflectivity geometry and gradients, mesocyclones and hook echoes, bounded weak echo regions, storm-top divergence, and reflectivity thresholds exceeding either specified heights or thermal levels (e.g., Browning and Donaldson 1963; Lemon 1977;

Supplemental information related to this paper is available at the Journals Online website: https://doi.org/10.1175/WAF-D-20-0083.s1.

Corresponding author: Charles Matthew Kuster, Charles.Kuster@noaa.gov

DOI: 10.1175/WAF-D-20-0083.1

Lemon and Doswell 1979; Moller et al. 1994; Brotzge and Donner 2013; Bowden et al. 2015; Liu et al. 2020). Therefore, the overall purpose of our work regarding Z_{DR} columns is to use rapid-update radar data to integrate this signature into some of these existing scientific conceptual models by comparing Z_{DR} column evolution to the evolution of other trusted radar signatures typically used during the warning decision process, such as upper-level reflectivity (Z) cores (e.g., Nelson 1983; Witt et al. 1998; Andra et al. 2002).

Our first attempt to integrate Z_{DR} columns into existing conceptual models—presented in Kuster et al. (2019)—used output from the Z_{DR} column depth algorithm (Snyder et al. 2015), which calculates the depth of the 1-dB Z_{DR} isosurface above the environmental 0°C level. In that study, an analysis of 42 storms in Oklahoma using output from this algorithm revealed that Z_{DR} column depth was a good discriminator between severe and nonsevere storms (with greater depths associated with severe storms), provided forecasters more time to issue warnings because its evolution preceded the evolution of −20°C reflectivity cores ($Z \geq 50$ dBZ), and provided a means to incorporate Z_{DR} columns into operational conceptual models. These results corroborated past work that showed strengthening Z_{DR} columns preceding increases in updraft intensity (e.g., Snyder et al. 2015) and hail cores at the surface (e.g., Picca et al. 2010; Kumjian et al. 2014).

These studies and work using the Z_{DR} column depth algorithm (Kuster et al. 2019) suggest that Z_{DR} columns could provide an early signal to forecasters that a storm is intensifying and may produce hazardous weather. However, the Z_{DR} column depth algorithm has limitations and requires additional development, so it will not be available to forecasters in real-time operations for at least several more years. Therefore, the purpose of this study is to explore whether or not the promising results of Kuster et al. (2019) hold for base data (e.g., Z and Z_{DR}) that are currently available to and used by forecasters during warning operations. Specifically, we performed a similar analysis and used nearly the same set of cases as Kuster et al. (2019) but only used base data products and analysis methods currently available to NWS forecasters to quantify the evolution of Z_{DR} column height and magnitude (sections 2 and 3) and relate that evolution to existing radar-focused conceptual models (section 4). Data analysis focused on determining typical characteristics of Z_{DR} columns (section 3a), differences between the Z_{DR} columns of tornadic and nontornadic mesocyclones (section 3b) as well as severe and nonsevere storms (section 3c). We also compared results using base data and Z_{DR} column depth algorithm output (section 3d) and examined the impact of radar volumetric update time on sampling Z_{DR} column evolution (section 3e).

2. Radar data and case information

All data used in this study were collected by a research WSR-88D (KOUN) located in Norman, Oklahoma. To approximate data from a future dual-pol phased array radar (e.g., Zrnić et al. 2007), we developed specialized volume coverage patterns (VCPs) and used 90° sector scans to obtain data with volumetric update times of 1.6–2.3 min. These VCPs typically contained about 10 elevation angles at heights primarily below 10 km above ground level (AGL) and nearly always sampled the full vertical extent of Z_{DR} columns. Elevation angles at higher heights were not included to allow for faster volumetric update times. Data quality was not sacrificed in these VCPs and was typically better than that available from operational WSR-88Ds due to the slower antenna rotation rate (12° s^{-1}) and resulting greater number of pulses per radial (128). This improved data quality may make it easier to identify and interpret Z_{DR} column evolution, but we expect that the differences are small enough as to not prevent the results presented below from being applied in an operational setting. From the available KOUN data collected over the past 7 years, we selected 45 storms from 13 events (each containing 2–8 storms), which provided 1308 volume scans of data for analysis (Table 1). We performed Z_{DR} calibration for all cases by inferring the presence of dry snow aggregates above the environmental melting layer similar to Picca and Ryzhkov (2012) and others.

TABLE 1. Total number of analyzed volume scans and individual storms for each storm type and severity. Within the single cell/multicell category is one tornadic quasi-linear convective system. This same storm's tornadic rotational signature is included in the tornadic mesocyclone category.

Storm type	No. of volume scans	No. of storms/mesocyclones
Supercell	730	20
Single cell/multicell	578	25
Severe	832	24
Nonsevere	476	21
Tornadic mesocyclone	274	9
Nontornadic mesocyclone	121	8

We used three different methods—all of which are available and relatively easy for forecasters to estimate in real time—to gather information about the height and magnitude of Z_{DR} columns. The maximum height AGL of the 1-dB isosurface within each Z_{DR} column was determined using vertical cross sections created by the Warning Decision Support System-Integrated Information software (Lakshmanan et al. 2007). We hereafter refer to this measure as "vertical cross-section height," and it can be reproduced by forecasters using either the Gibson Ridge (GR) radar viewing software or the Four-Dimensional Stormcell Investigator (FSI) tool within the Advanced Weather Interactive Processing System (AWIPS). To obtain another measure of Z_{DR} column height and magnitude, we also measured the maximum height AGL of ≥1-dB Z_{DR} on any elevation angle's planned position indicator (PPI) as well as the maximum value of Z_{DR} at this elevation angle. We hereafter refer to these measures as "PPI height" and "max column-top Z_{DR}," respectively, and both can be determined quickly by forecasters using AWIPS or GR. It is important to note that vertical cross-section height uses height information from the top of a radar beam while PPI height uses height information from the middle of a radar beam and that GR provides height as above radar level (ARL) while AWIPS can provide height as AGL or ARL. "Raw" (i.e., not

"smoothed" or recombined) Z_{DR} data were used for all analyses. We did not calculate any measure of Z_{DR} column size—despite it likely being a useful characteristic (e.g., Van Den Broeke 2017; Kuster et al. 2019)—because such a calculation in real time would require an automated algorithm that is not yet available to forecasters issuing warnings. No automated filtering was performed on the Z_{DR} data to remove noise and errors, but if clearly erroneous Z_{DR} values (e.g., excessively high values) were seen, they were ignored during the analysis process. This manual filtering was not required frequently, and forecasters could do the same by ignoring erroneous Z_{DR} values during operations.

One important limitation for forecasters to consider when determining the height or magnitude of a Z_{DR} column using these metrics is the vertical spacing between consecutive elevation angles of the radar data. For example, if the actual ≥1-dB Z_{DR} column extends to just below a given elevation angle, it is likely that Z_{DR} column height will be underestimated. The extent of this limitation also changes as a storm's range from the radar changes and will be greater at longer ranges. This limitation can cause artificial "jumps" up or down in Z_{DR} column height as the storm moves toward or away from the radar. In this study, no normalization based on range was performed to account for these artifacts since no such processing occurs in real-time warning operations, but the large sample size may help reduce the artifacts' overall effects on the results. In addition, to help minimize limitations arising from reduced vertical data coverage (i.e., vertical distance between the beam heights of two consecutive elevation angles) and beam broadening, all analyzed storms were within 150 km of KOUN, all but one were within 120 km, and a vast majority were within 100 km. For operations, the use of VCPs with the highest possible vertical data coverage would likely help alleviate this limitation.

3. Radar data analysis and results

All storms used in this analysis were classified as severe or nonsevere while all supercell mesocyclones were classified as tornadic or nontornadic based on a manual determination of whether or not each storm or mesocyclone was associated with a severe weather report (i.e., wind, hail, or tornado) in the National Center for Environmental Information's Storm Events Database at any point in their lifetime (i.e., radar data analysis window ± 30 min). Despite our best efforts to quality control the data, there are known limitations when using storm reports (e.g., Trapp et al. 2006), but this option provides the best available means for classifying storms in this study. All results presented here are from an analysis of 1308 volume scans spanning storms with varying modes and intensities (Table 1) that occurred at different times of the year (April–October), so the results could be applicable to a relatively wide range of operational situations. However, because all analyzed storms occurred in central Oklahoma during the warm season, readers and forecasters should be cautious of applying these results in environments and storm modes not commonly seen in the Southern Great Plains as well as in cold-season events.

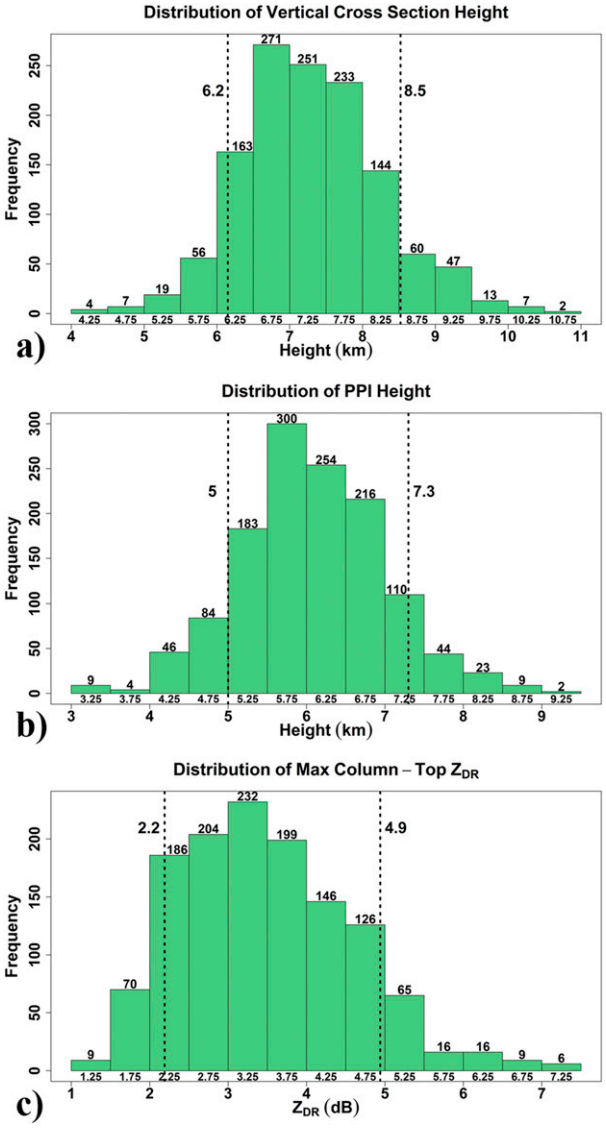

FIG. 1. Distribution of (a) vertical cross-section height, (b) PPI height, and (c) max column-top Z_{DR} for all volume scans (n = 1308) considered. Bin midpoints and counts are included below and above each column, respectively. Vertical dashed lines indicate the 10th and 90th percentiles.

a. *Typical Z_{DR} column characteristics*

An important first step in understanding Z_{DR} columns in the context of scientific conceptual models is an awareness of what magnitudes and trends may be typical for the signature. Vertical cross-section height was typically (hereafter defined as 80% of the volume scans) between 6.2 and 8.5 km AGL, PPI height was typically between 5.0 and 7.3 km AGL, and max column-top Z_{DR} was typically between 2.2 and 4.9 dB (Fig. 1).

Forecaster knowledge of how Z_{DR} columns change on short time scales may also be important information. There were many small changes in Z_{DR} column height and magnitude (i.e., max column-top Z_{DR}) that may not prove meaningful for a

storm's severe weather potential. Focusing on the more significant changes may be most important for anticipating storm intensification and potential hazards. We therefore examined how Z_{DR} columns changed over all instances of successive five rapid-update volume scans (about 10 min) to see what trends forecasters could expect. This time period was chosen because Z_{DR} columns tend to intensify to relative peaks or weaken over a period of about 10 min and many warning decisions are made in 10 min or less. Our analysis showed that if looking at a random point during Z_{DR} column evolution, it was nearly as likely that Z_{DR} column height or magnitude would increase as decrease over the 10-min period (Fig. 2). Therefore, it is important to be aware of trends (i.e., is the Z_{DR} column strengthening or weakening). If the Z_{DR} column is intensifying, looking for greater increases in height or magnitude over the next 10 min (i.e., 75th percentile; dashed lines in Fig. 2) could alert a forecaster that the storm's updraft is significantly strengthening and could therefore produce hazardous weather soon. For example, an increase in a Z_{DR} column's cross-section height of 0.7 km in 10 min or less could be more relevant to a forecaster diagnosing severe potential than a change of only 0.25 km (Fig. 2a).

b. Z_{DR} column characteristics of tornadic and nontornadic mesocyclones

Knowing these typical ranges of Z_{DR} column height and magnitude could be important since we observed differences between the Z_{DR} columns of tornadic and nontornadic mesocyclones as well as severe and nonsevere storms (section 3c). To determine statistical significance between any two distributions and their medians, we used two different methods for completeness: 1) two-sample Kolmogorov–Smirnov (K–S) tests and 2) a bootstrapping method with replacement (n = 10 000). If the K–S test p values were <0.05 or if the observed differences in the medians of two distributions were greater than the 95th percentile of the simulated differences using the bootstrapping method, the differences were considered statistically significant.

In comparing the volume scans of tornadic (n = 274) and nontornadic (n = 121) mesocyclones, distributions of vertical cross-section height and PPI height showed statistically significant differences, but distributions of max column-top Z_{DR} did not (Table 2). However, the differences were much smaller—with only the distribution of vertical cross-section height showing statistically significant differences—when only looking at times when a mesocyclone was producing a tornado compared to when it was not (not shown). In addition, we observed no clear differences in the distributions of Z_{DR} column height or magnitude between mesocyclones associated with tornadoes with different ratings on the enhanced Fujita scale. That is, Z_{DR} column characteristics were generally similar for mesocyclones that produced an EF0 tornado or an EF4 tornado. These results differ from Van Den Broeke (2017, 2020) who had a larger sample size (n = 35 tornadic, 32 pretornadic, and 31 nontornadic storms) than this study (n = 10 tornadic and 11 nontornadic storms), so any potential relationship between Z_{DR} columns and tornadoes deserves further investigation. In this study, we focus primarily on Z_{DR} columns relative to severe and nonsevere storms since the differences in the distributions are more robust (section 3c) and there is more research linking Z_{DR} columns with updrafts and severe hail (e.g., Kumjian and Ryzhkov 2008; Picca et al. 2010; Kumjian et al. 2014; Kuster et al. 2019) than there is linking Z_{DR} columns to tornadogenesis.

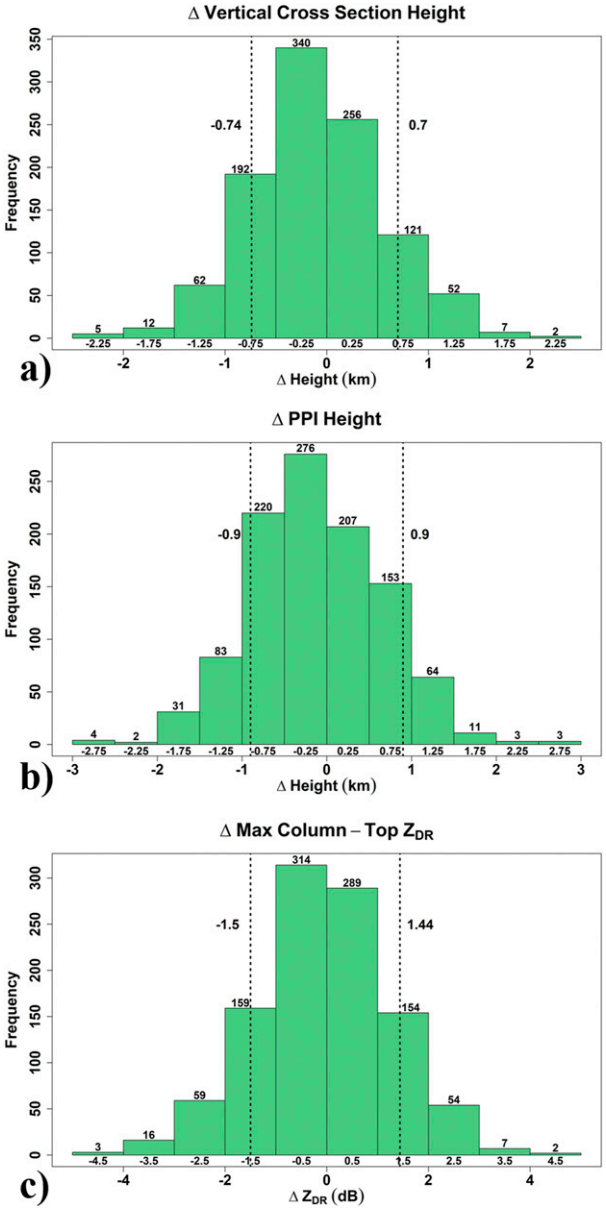

FIG. 2. Distribution of changes (i.e., delta) in (a) vertical cross-section height, (b) PPI height, and (c) max column-top Z_{DR} over five rapid-update volume scans (about 10 min). Bin midpoints and counts are included below and above each column, respectively. Vertical dashed lines indicate the 25th and 75th percentiles.

c. Z_{DR} column characteristics of severe and nonsevere storms

In this dataset, statistically significant differences were common between the distributions of Z_{DR} column height and

TABLE 2. Statistical significance using a bootstrapping method with replacement and K–S test p values for various radar metrics across all volume scans (n = 1308). Metrics with observed differences larger (in magnitude) than the 95th percentile bootstrapping method differences or with K–S test p values < 0.05 were considered statistically significant and are indicated by two asterisks (**).

Radar signature metric	95th percentile bootstrapping differences	Observed difference in radar signature median	K–S test p value
Tornadic vs nontornadic mesocyclone			
Vertical cross-section height**	210 m	665 m	<0.01
PPI height**	200 m	700 m	<0.01
Max column-top Z_{DR}	0.31 dB	−0.13 dB	0.11
Z_{DR} column depth algorithm max (Kuster et al. 2019)	−124 m	−53 m	0.33
Severe vs nonsevere thunderstorm			
Vertical cross-section height**	150 m	685 m	<0.01
PPI height**	200 m	500 m	<0.01
Max column-top Z_{DR}**	0.13 dB	0.50 dB	<0.01
Z_{DR} column depth algorithm max (Kuster et al. 2019)**	131 m	549 m	<0.01

magnitude when comparing the volume scans of severe (n = 832) and nonsevere (n = 476) storms. The differences between the distributions of vertical cross-section height, PPI height, and max column-top Z_{DR} were all statistically significant, and vertical cross-section height provided the largest differences between severe and nonsevere storms (Fig. 3; Table 2). These statistically significant differences were also observed when breaking down the dataset by storm mode (i.e., considering supercells and single/multicells separately) except for PPI height between severe and nonsevere multicells (not shown).

Despite the statistically significant differences, the distributions of Z_{DR} column characteristics between severe and nonsevere storms still overlap, potentially making it more challenging for warning forecasters to use Z_{DR} columns to inform warning decisions. One potentially helpful metric to consider is how many volume scans were associated with severe and nonsevere storms at various thresholds of Z_{DR} column height and magnitude. For example, once vertical cross-section height reached 7.5 km, at least 70% of the volume scans in this study were associated with severe thunderstorms (Fig. 4). Similarly, once max column-top Z_{DR} reached 4.5 dB, at least 70% of the volume scans in this study were associated with severe storms. It is important to remember, however, that many volume scans associated with severe storms in this study occurred below these thresholds, so they cannot be used as a singular warning trigger. Other information—including environmental information and other radar metrics—must also be used to make warning decisions, but Z_{DR} columns could provide forecasters with another piece of information to increase confidence in either issuing or not issuing a warning.

Another way of looking at the data involves only considering the maximum value of Z_{DR} column height or magnitude for each storm (n = 45) rather than considering Z_{DR} column height or magnitude for every volume scan (n = 1308) associated with a storm, as was done above. This method provides a summary of maximum Z_{DR} column height and magnitude seen across the dataset. We did not focus on this method because it provides only a snapshot of a storm at its highest intensity and, more importantly, forecasters look at a storm volume scan by volume scan in real time rather than evaluating the entire storm's evolution in hindsight. When looking at each storm's maximum value of Z_{DR} column height and magnitude, severe storms still had taller Z_{DR} columns with greater Z_{DR} values than nonsevere storms in general, especially when looking at cross-section height and column-top Z_{DR} (Fig. 5). The biggest difference, compared to the volume scan by volume scan approach, is that these differences are only statistically significant for column-top Z_{DR}, perhaps due to the smaller number of data points used in determining statistical significance. Still, the differences in the distributions could give forecasters additional information to use when interrogating a storm's Z_{DR} column especially if that Z_{DR} column exhibits characteristics typically only seen with severe storms in this dataset (e.g., a cross-section height of ≥8.5 km).

d. *Comparison with Z_{DR} column depth algorithm results*

Since the analysis conducted on radar base data and the Z_{DR} column depth algorithm (presented in Kuster et al. 2019) is very similar in terms of cases, analysis techniques, and participating scientists, this dataset provides a unique opportunity to compare information available via base data and algorithm output. In general, many of the results were similar when using base data and Z_{DR} column depth algorithm output: Z_{DR} columns provide information about a storm's potential severity, evolve prior to −20°C reflectivity cores, and generally occur prior to severe hail and wind reports. Statistical significance was comparable between algorithm output and base data analysis, and all metrics had clear statistical significance between severe and nonsevere storms (Table 2).

One difference between the two datasets relates to the Z_{DR} column characteristics of tornadic and nontornadic mesocyclones. When looking at Z_{DR} columns in base data, there were statistically significant differences in the distributions of two different metrics (section 3b). However, there were no statistically significant differences between the Z_{DR} column depth algorithm output of tornadic and nontornadic mesocyclones (Kuster et al. 2019). We are unsure why this difference exists, though the algorithm is designed to provide output without subjective assessment, so additional filtering occurs in the algorithm to reduce false detections of Z_{DR} columns. In contrast, subjectively determined Z_{DR} column characteristics using base data, as reported here, may be less affected by data quality

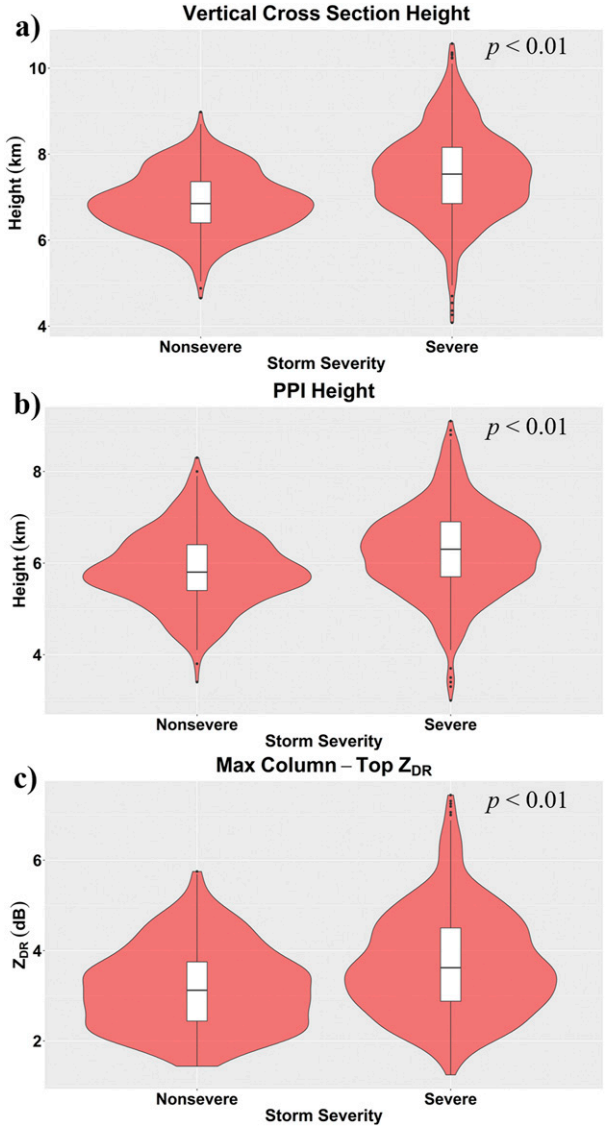

FIG. 3. Violin plots of (a) vertical cross-section height, (b) PPI height, and (c) max column-top Z_{DR} for all volume scans (n = 1308) considered. The red area shows the probability density with a greater width indicating a higher frequency of occurrence. Associated box plots are included within each violin plot for reference. Box edges are the lower (Q1) and upper (Q3) quartiles, the horizontal black line is the median, and outliers are indicated by black dots. K–S test p values are also included.

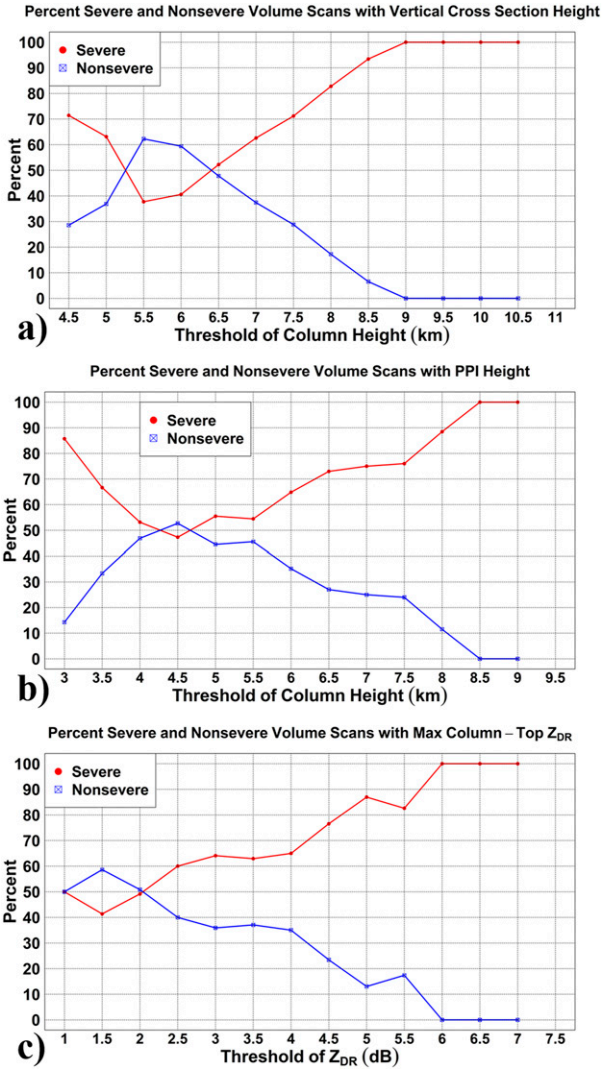

FIG. 4. Percent of all volume scans for severe (red line) and nonsevere (blue line) storms for (a) vertical cross-section height, (b) PPI height, and (c) max column-top Z_{DR}.

issues (e.g., noise, erroneous pixels, etc.) because the well-trained human behind the assessment can adjust for such issues. Regardless, the differences in the statistical significance of tornadic and nontornadic mesocyclones when using Z_{DR} column depth algorithm output and when using base data highlight the uncertainty regarding the connection, if any exists, between Z_{DR} column characteristics and tornadoes.

The biggest difference between the two datasets occurred with the lag correlation analysis. In both studies, we calculated lag correlations between each signature and then determined statistical significance using a bootstrapping method with replacement (n = 5000). Lag correlations were higher when using algorithm output and had more consistent statistical significance than all the base data metrics (Figs. 6a,b). The most likely reason for this observation is the reduced variability associated with the algorithm output compared to the base data especially when considering Z_{DR} column size (i.e., cross-sectional area). This lower variability is illustrated by the slower reduction in the autocorrelation function of Z_{DR} column size indicated by the Z_{DR} column depth algorithm output compared to the vertical cross-section height (Figs. 6c,d). Therefore, outside of presenting Z_{DR} column information in a more concise way than base data, the Z_{DR} column depth algorithm appears beneficial in the sense that data output likely contains more volume scan to volume scan consistency and less noise overall than base data likely due to the filtering and

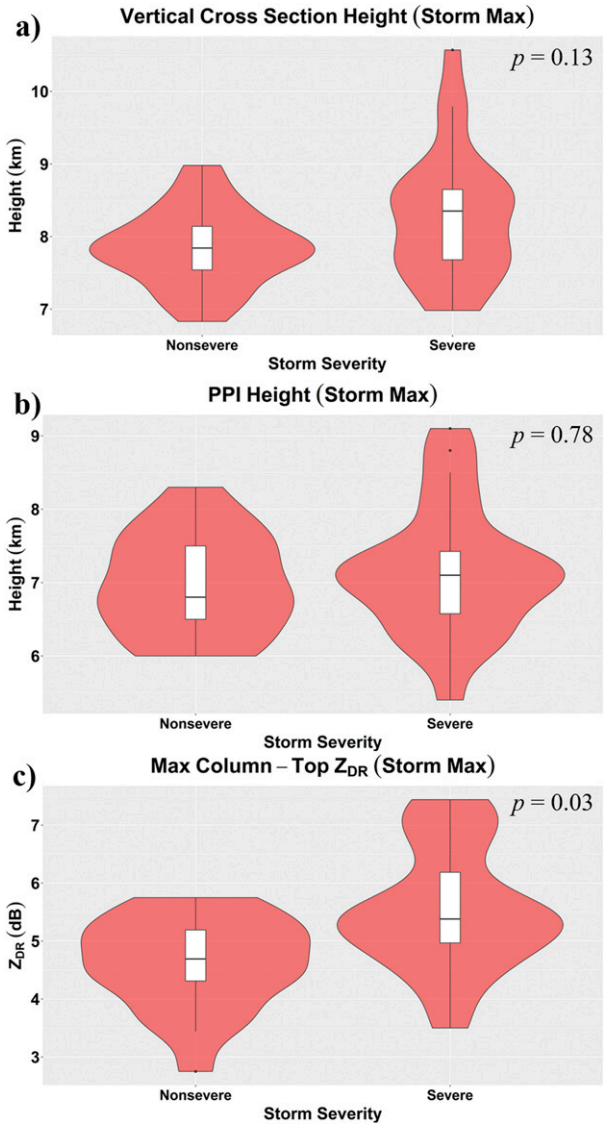

FIG. 5. Violin plots of (a) vertical cross-section height, (b) PPI height, and (c) max column-top Z_{DR} for a single maximum value associated with each storm (n = 45). The red area shows the probability density with a greater width indicating a higher frequency of occurrence. Associated box plots are included within each violin plot for reference. Box edges are the lower (Q1) and upper (Q3) quartiles, the horizontal black line is the median, and outliers are indicated by black dots. K–S test p values are also included.

interpolation used by the algorithm. The transition of this algorithm to operations may provide valuable information for forecasters pending further development and refinement, but it is encouraging that base data can also be used to obtain operationally relevant information.

e. Impacts of volumetric radar update time

All results discussed so far used rapid-update KOUN data with volumetric update times of no more than 2.3 min. To examine what impact radar update time might have on the results, we also degraded the KOUN data (i.e., retained only every third volume scan) to simulate radar data with a volumetric update time of 5–7 min, which is relatively close to the current volumetric update time of operational WSR-88Ds. We then performed similar analyses on the degraded data that we did with the unaltered KOUN data and compared the results. In general, the results between the two datasets were similar, which suggests the results of this study are applicable in operations at the currently available WSR-88D volumetric update times.

There were, however, a few subtle differences that point toward benefits of observing Z_{DR} columns with rapidly scanning radars. For example, the differences in the distributions of Z_{DR} column height and magnitude between severe and nonsevere storms as well as tornadic and nontornadic mesocyclones were somewhat smaller for the degraded data than for the unaltered data. All K–S test p values for severe and nonsevere storms using the degraded data were still statistically significant, but they were larger (i.e., less significant) than those of the unaltered rapid-update data.

This difference may arise from rapid changes in Z_{DR} column characteristics that could cause local maxima of Z_{DR} column height and magnitude to be missed because they occur between WSR-88D volume scans. Less frequent updates may also make it more challenging for forecasters to understand Z_{DR} columns in the context of their conceptual models (section 4) since a more complete evolutionary picture is not available to them. For example, on 8 July 2014, degraded KOUN data depicted a period of Z_{DR} column strengthening and subsequent weakening later and with less detail than the unaltered KOUN data (Fig. 7). Having a more complete understanding of the changes in Z_{DR} column strength provided here by rapid-update (i.e., unaltered) data could help a forecaster more efficiently recognize the presence of an updraft pulse and diagnose the hazardous weather it could produce.

4. Z_{DR} columns and scientific conceptual models

Perhaps the most important aspect of using a new radar signature in the warning decision process is a thorough understanding of what a signature's evolution is revealing about storm-scale structure and processes and successful incorporation of information provided by the signature into one's severe-weather conceptual model. Previous research has shown that Z_{DR} columns are strongly related to a storm's updraft intensity. Kumjian et al. (2014) used numerical simulations to show that the height of the 2-dB Z_{DR} isosurface was strongly correlated with an updraft's vertical velocity at that height, while Snyder et al. (2015) also used numerical simulations to show that the deepest Z_{DR} columns were associated with the most intense updrafts. Since updraft strength is typically linked with the magnitude of a storm's hazardous weather (e.g., Nelson 1983; Johns and Doswell 1992; Kumjian and Ryzhkov 2008; Picca et al. 2010; Kumjian 2013), the use of Z_{DR} columns could provide important information to forecasters.

Here, we provide examples of what Z_{DR} column evolution could mean in the context of scientific conceptual models and

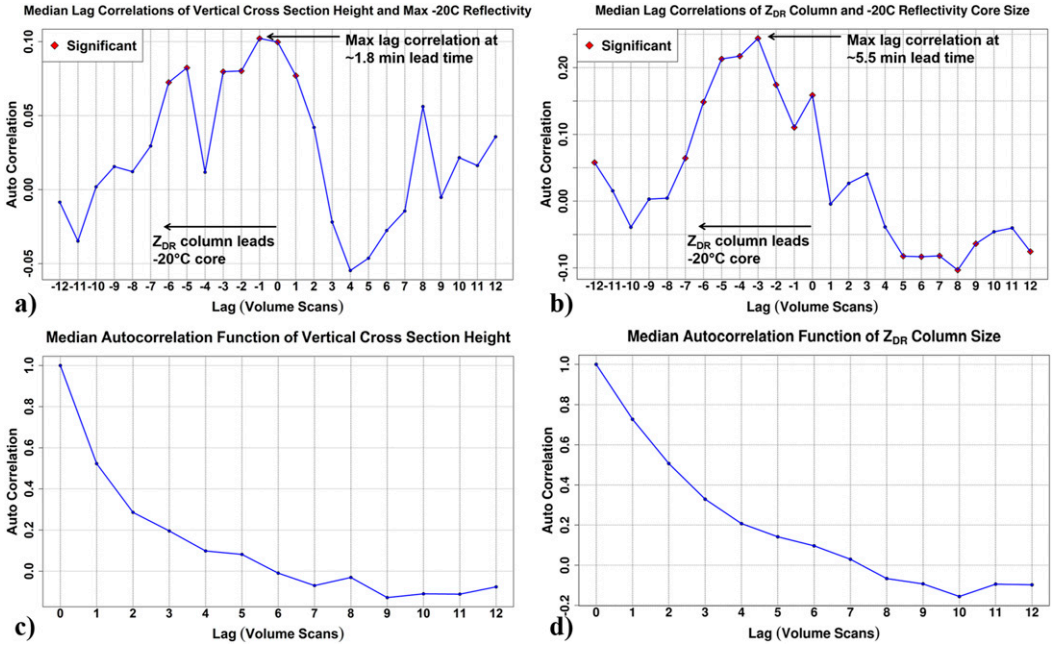

FIG. 6. Median lag correlations between (a) vertical cross-section height and maximum −20°C reflectivity and (b) Z_{DR} column depth size and −20°C reflectivity core size, and median autocorrelation function of (c) vertical cross-section height and (d) Z_{DR} column depth size. (left) The base data and (right) Z_{DR} column depth algorithm output. In (a) and (b), red markers indicate statistical significance (95% confidence) and positive correlations at negative lag times indicate that Z_{DR} column evolution precedes −20°C reflectivity core evolution.

show relationships between the Z_{DR} column and other radar signatures, such as −20°C reflectivity cores, that forecasters may use during the warning decision process. Our analysis shows that Z_{DR} columns typically develop and evolve prior to upper-level (e.g., −20°C) reflectivity cores, which corroborates previous research (e.g., Knight 2006; Snyder et al. 2015). We used lag correlations (section 3d) to quantify this relationship and found that vertical cross-section height provides the most consistent signal—likely due to its lower volume scan to volume scan variability compared to the other two metrics (not shown)—in terms of Z_{DR} column evolution preceding −20°C reflectivity core evolution (Fig. 8). Positive lag correlations at negative lag times suggest that Z_{DR} column evolution leads −20°C reflectivity core evolution. For example, if we assume an average volumetric update time of 1.8 min for KOUN across all cases, a lag of −4 volume scans in Fig. 8a represents a lag time of about 7 min.

Therefore, based on results from these cases, a forecaster seeing an increase in Z_{DR} column vertical cross-section height could expect to see an increase in −20°C reflectivity core magnitude in the next ~11 min (Fig. 8a). PPI height and max column-top Z_{DR} also showed similar lag correlation patterns, but they were either more variable or had lower correlation values (Figs. 8b,c). This evolution fits well with existing conceptual models because Z_{DR} columns are typically associated with developing updrafts and enhanced positive Z_{DR} can be present very shortly after an updraft develops, whereas upper-level reflectivity cores are typically associated with greater concentrations of hailstones and large freezing rain drops that develop later as the result of an updraft (e.g., Knight 2006; Kumjian et al. 2014).

One clear example of this time separation occurred with a downburst-producing multicell thunderstorm on 8 July 2014 (Fig. 9). In this case, a robust Z_{DR} column with $Z_{DR} > 4$ dB developed by 2252:29 UTC, before a collocated −20°C reflectivity core was present (Fig. 9a). The Z_{DR} column then grew and intensified through 2258:40 UTC (Figs. 9a–d). About 10.5 min after robust Z_{DR} column development, a strong −20°C reflectivity core with $Z > 50$ dBZ developed at 2302:48 UTC and then grew and intensified through about 2311:01 UTC (Figs. 9f–j). Here, a forecaster using Z_{DR} would be aware of the development of a potentially strong new updraft earlier than if using reflectivity alone. With the knowledge of strong updraft development, a forecaster could begin to consider other factors, including the near-storm environment and relevant conceptual models, and perhaps anticipate an increase in hail, strong winds, and/or precipitation intensity at the surface before high reflectivity develops aloft.

A similar example occurred with a downburst-producing multicell thunderstorm on 10 July 2013. In this case, a robust Z_{DR} column with Z_{DR} near 4 dB developed by 2029:36 UTC (Fig. 10a) or about 13.5 min prior to the development of a −20°C reflectivity core with $Z > 50$ dBZ at 2043:15 UTC (Fig. 10g) and about 20.5 min prior to a severe wind report of 52 kt (26.8 m s^{-1}) at 2050 UTC (Fig. 10j). Similar to the previous case, use of Z_{DR} would signal to a forecaster that a strong updraft was developing before a −20°C reflectivity core appeared. Additionally, relative increases in Z_{DR} column height

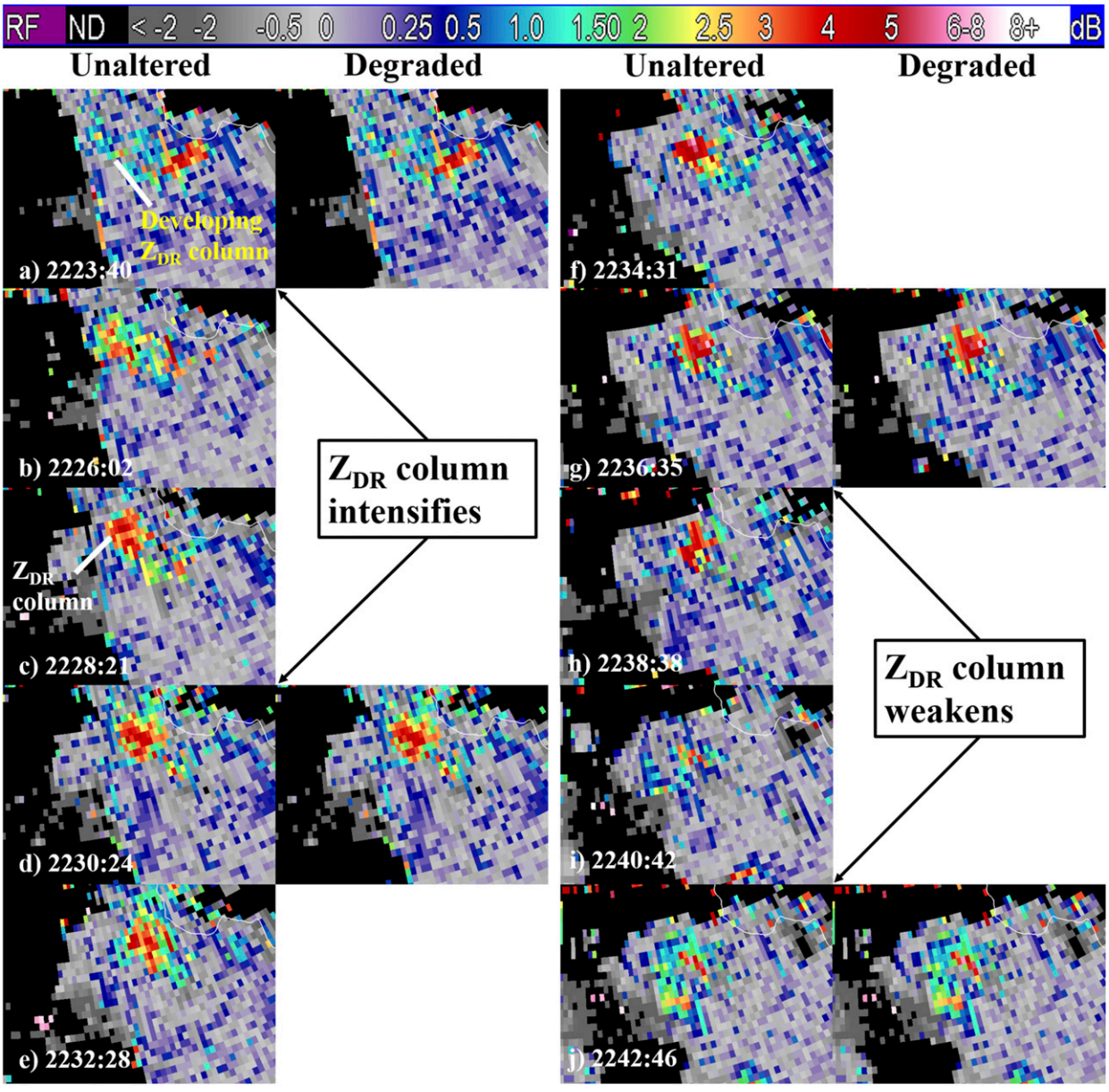

FIG. 7. (left) Unaltered and (right) degraded KOUN data for a Z_{DR} column between (a) 2223:40 and (j) 2242:46 UTC 8 Jul 2014. Unaltered data represents rapid-update data (about 2-min volumes) and degraded data represents traditional-update data (about 6-min volumes). All images are from the 7.9° elevation angle (about 4.6 km AGL). Storm range from radar is about 33 km. Color bar for Z_{DR} (dB) is located at the top. See the online supplemental material for an animation of this figure.

and magnitude are more obvious than increases in −20°C reflectivity core magnitude (Fig. 10), which could help a forecaster better understand that a stronger updraft ''pulse'' was occurring. Using this additional information about the storm's updraft could suggest that hazards such as hail or strong winds are possible (e.g., Johns and Doswell 1992; Kumjian 2013).

The Z_{DR} column evolution is also applicable to conceptual models of updrafts associated with other storm modes such as supercells. In several cases, we observed Z_{DR} column development or intensification (i.e., increase in magnitude or areal extent of Z_{DR} column) prior to the development of a bounded weak echo region (BWER), which is another radar signature forecasters can use to infer the existence of a strong updraft (e.g., Krauss and Marwitz 1984; Lakshmanan and Witt 1997). One particularly clear example of this evolution occurred on 31 May 2013 when a robust Z_{DR} column with $Z_{DR} > 4$ dB formed by 2248:43 UTC (Fig. 11a). This Z_{DR} column developed about 10 min prior to the development of a BWER in the −20°C reflectivity field (Fig. 11d) and about 16 min prior to a report of 5.9 in. (15.0 cm) diameter hail at 2305 UTC.

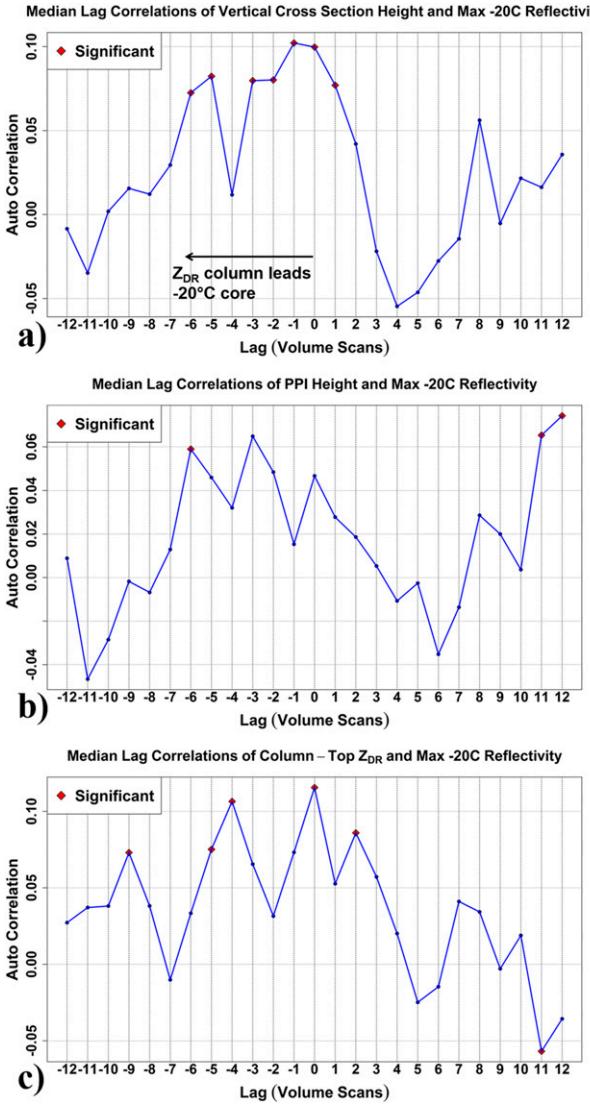

FIG. 8. Median lag correlations between (a) vertical cross-section height and maximum −20°C reflectivity, (b) PPI height and maximum −20°C reflectivity, and (c) maximum column-top Z_{DR} and maximum −20°C reflectivity. Red markers indicate statistical significance (95% confidence), and positive correlations at negative lag times indicate that Z_{DR} column evolution precedes −20°C reflectivity core evolution.

After robust development at 2248:43 UTC, the Z_{DR} column continued to grow and eventually evolved into a ring-like shape (e.g., Kumjian and Ryzhkov 2008) at about the same time the BWER developed (Figs. 11a–e). Once again, Z_{DR} column evolution could provide information about a storm's updraft earlier than features observed in reflectivity. Therefore, use of Z_{DR} columns—and conceptual models that include them—could provide forecasters with more time to issue warnings and increase confidence in issuing those warnings.

In addition to Z_{DR} columns strengthening prior to −20°C reflectivity cores and severe hail reports in supercells, changes in Z_{DR} column magnitude may also be easier to observe than changes in −20°C reflectivity. One such example occurred on 19 May 2013. A robust Z_{DR} column with $Z_{DR} > 4$ dB was common with this storm, but the column did undergo a brief period of weakening around 2353:20 UTC, which likely indicated that the storm was temporarily weaker around this time (Fig. 12a). By 2359:22 UTC, a stronger Z_{DR} column with $Z_{DR} > 4$ dB was once again present (Fig. 12d). It then continued to increase in magnitude and was especially strong between 0007:56 and 0016:12 UTC, or about 8–16 min prior to a report of 1.0 in. (2.5 cm) diameter hail at 0024 UTC (Figs. 12f–i). In contrast to the Z_{DR} column, after weakening between 2356:21 and 0002:26 UTC, the −20°C reflectivity core did not exhibit any clear changes in magnitude after 0002:26 UTC (Figs. 12b–j). Therefore, in addition to revealing information about a storm's updraft characteristics to forecasters earlier than −20°C reflectivity, it is also possible that it is easier to infer changes in updraft intensity when using Z_{DR} columns especially when high (e.g., 50+ dBZ) −20°C reflectivity is widespread and any changes in magnitude are relatively subtle. In this case, −20°C reflectivity suggested the storm was relatively steady state if not weakening, but an examination of Z_{DR} columns revealed the occurrence of a clear updraft pulse that likely resulted in severe hail at the surface.

5. Summary

Dual-pol radar data provide new information that can help forecasters understand storm-scale processes, yet these data are likely not seeing widespread use in the warning decision process. The goal of this study is to provide information to forecasters about Z_{DR} columns relative to severe weather warnings and scientific conceptual models using base data that are currently available in a real-time operational environment. We examined base data to determine a Z_{DR} column's 1-dB vertical cross-section height, maximum height indicated by PPIs, and maximum column-top Z_{DR} for a wide variety of storm modes and environments. From this analysis of 45 storms in Oklahoma, we conclude the following:

1) Statistically significant differences exist between the distributions of Z_{DR} column height and magnitude for severe and nonsevere storms with severe storms having taller and stronger Z_{DR} columns. Less certainty exists when it comes to differences between tornadic and nontornadic mesocyclones, in part due to our relatively small sample size, but statistically significant differences did exist between the distributions of Z_{DR} column height for tornadic and nontornadic mesocyclones, with tornadic mesocyclones having taller Z_{DR} columns.
2) In general, Z_{DR} columns develop and intensify prior to −20°C reflectivity core development and intensification as well as other reflectivity signatures such as BWERs. Using this information to integrate Z_{DR} columns into existing storm interrogation methods and scientific conceptual models could allow forecasters to anticipate changes in storm intensity and radar signatures already used to make warning decisions (e.g., upper-level reflectivity cores), which could help increase warning confidence and lead time.

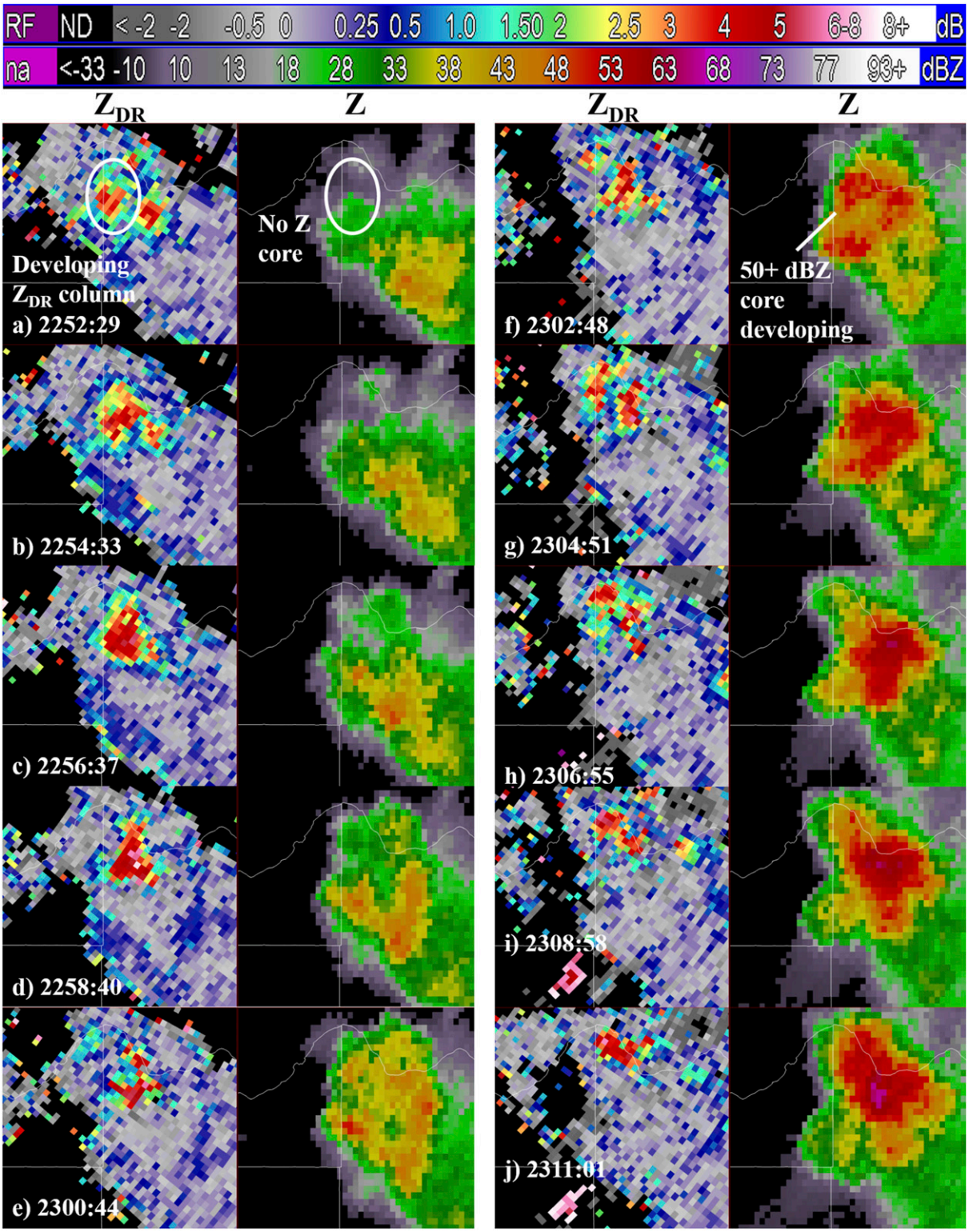

FIG. 9. (left) Z_{DR} and (right) −20°C reflectivity for every volume scan between (a) 2252:29 and (j) 2311:01 UTC 8 Jul 2014. The Z_{DR} images are from the 4.10° elevation angle (about 4.6 km AGL). The −20°C height is about 7.5 km AGL. Storm range from radar is about 60 km. Color bars for Z_{DR} (dB) and −20°C reflectivity (dBZ) are included at the top. See the online supplemental material for an animation of this figure.

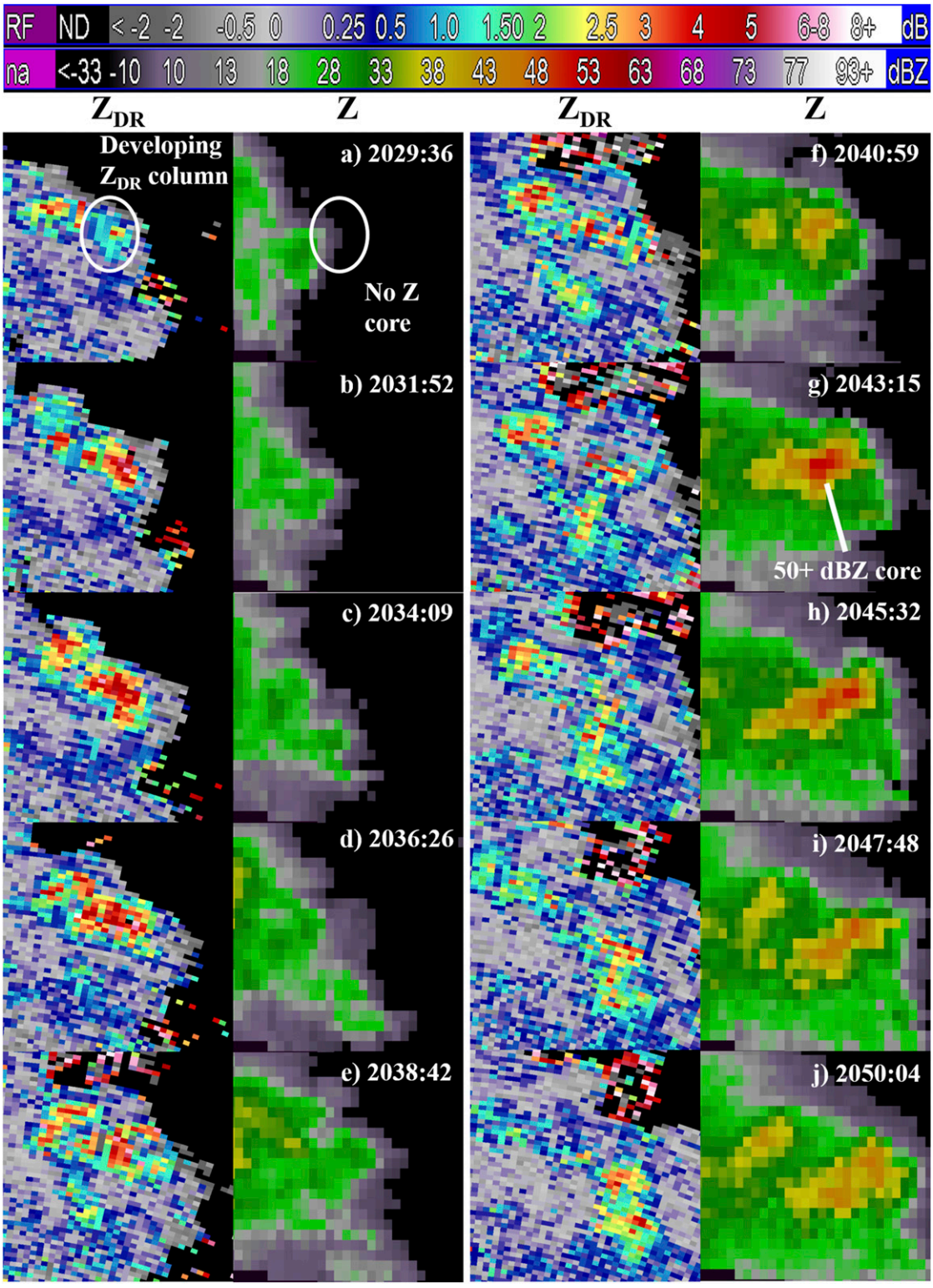

FIG. 10. (left) Z_{DR} and (right) −20°C reflectivity for every volume scan between (a) 2029:36 and (j) 2050:04 UTC 10 Jul 2013. The Z_{DR} images are from the 6.0° elevation angle (about 4.9 km AGL). The −20°C height is about 7.9 km AGL. Storm range from radar is about 45 km. Color bars for Z_{DR} (dB) and −20°C reflectivity (dBZ) are included at the top. See the online supplemental material for an animation of this figure.

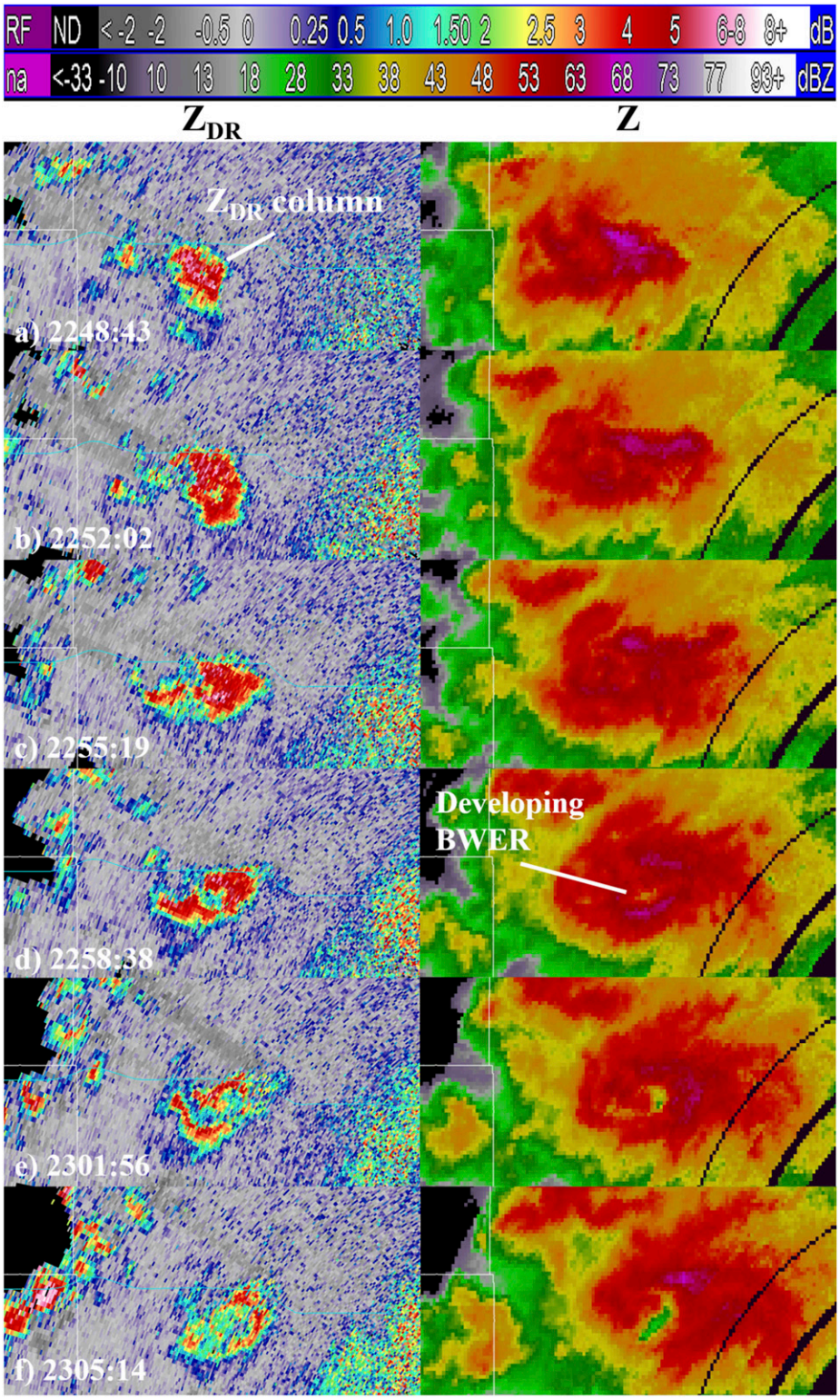

FIG. 11. (left) Z_{DR} and (right) −20°C reflectivity for every other volume scan between (a) 2248:43 and (j) 2305:14 UTC 31 May 2013. The Z_{DR} images are from the 4.05° elevation angle and range from about 4.9 km AGL in (a) to 4.5 km AGL in (f). The −20°C height is about 6.9 km AGL. Storm range from radar is from about 66 km in (a) to 61 km in (f). Color bars for Z_{DR} (dB) and −20°C reflectivity (dBZ) are included at the top. See the online supplemental material for an animation of this figure.

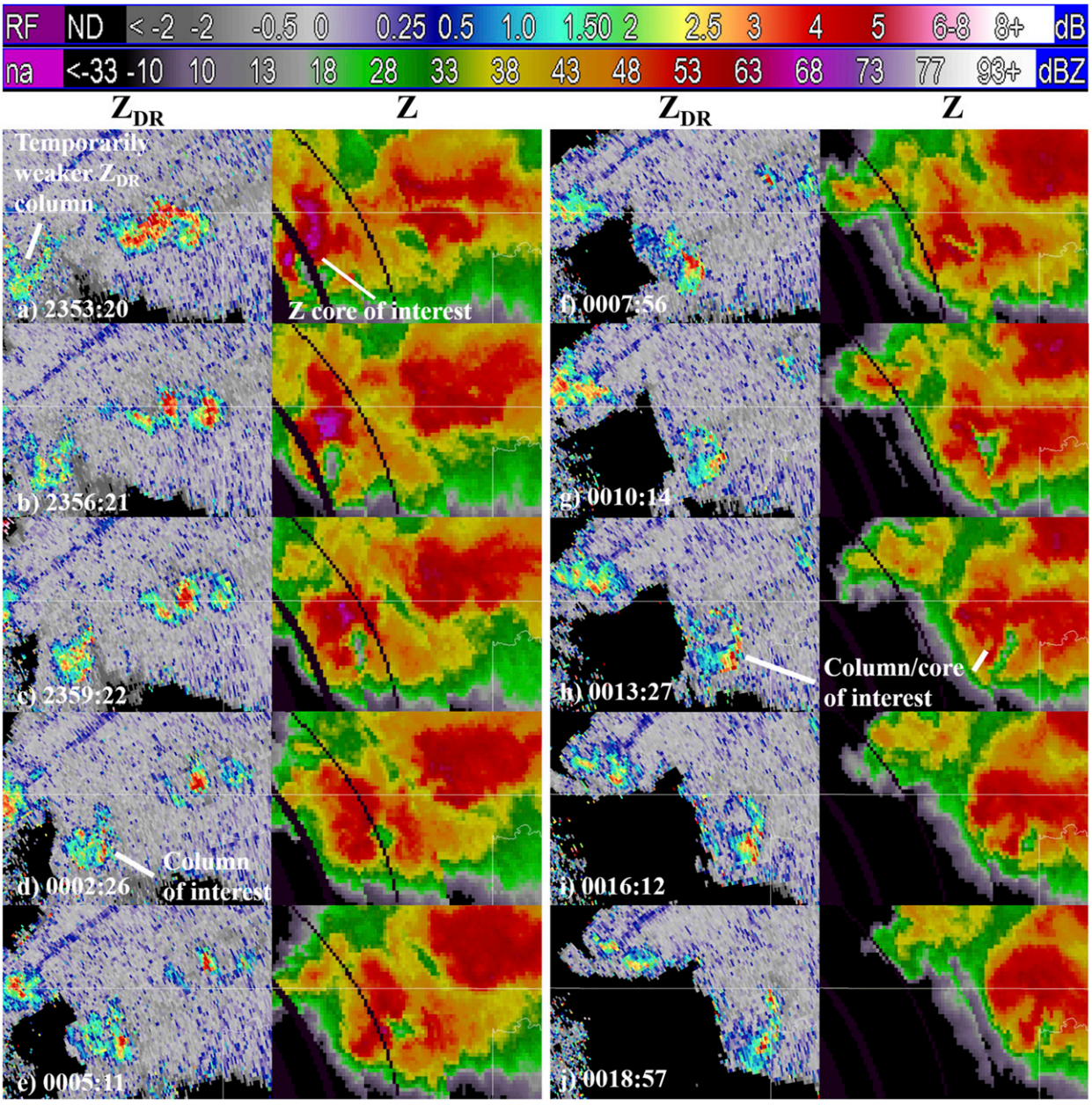

FIG. 12. (left) Z_{DR} and (right) −20°C reflectivity for every other volume scan between (a) 2353:20 and (j) 0018:57 UTC 19–20 May 2013. Z_{DR} images are from the 5.05° elevation angle and range from about 3.3 km AGL in (a) to 5.9 km AGL in (j). The −20°C height is about 6.8 km AGL. Storm range from radar is about 37 km in (a) to 64 km in (j). Color bars for Z_{DR} (dB) and −20°C reflectivity (dBZ) are included at the top. See the online supplemental material for an animation of this figure.

3) Results using base data and output from the Z_{DR} column depth algorithm were generally similar, but the algorithm does appear to be advantageous especially in terms of reduced variability and noise, so pursuing development and transition of the algorithm to operations may benefit forecasters.
4) Rapid-update radar data allow for a more complete evolutionary understanding of Z_{DR} columns, which can increase statistical differences between the Z_{DR} column characteristics of severe and nonsevere storms and aid forecasters in incorporating this signature into their conceptual models. However, all results presented here are still applicable in operations today because statistically significant results were observed using the degraded KOUN data that has a similar update time to the current WSR-88D network.

Considering these results in the context of conceptual models, such as the role of updrafts in severe weather and what

radar can reveal about these updrafts, is likely important for improved understanding of storm-scale processes and improved warning performance and to address some of the limitations inherent in this study and in radar data itself. Despite using a wide range of storm modes and environments, all analyzed storms were in Oklahoma, so the results may not be applicable across all geographic regions. These results also apply generally to storms that are within 100 km of a WSR-88D. Radar sampling—both spatial and temporal—is likely to impact the ability to use Z_{DR} columns to inform conceptual models or warning decisions. At greater ranges, not only is the radar beam larger but the vertical resolution and data coverage also decreases. These factors decrease the precision and accuracy of estimating a storm's exact Z_{DR} column height and magnitude. However, using available data and applying robust conceptual models could help a forecaster gain information about a storm's updraft and aid in the anticipation of severe weather at the surface. There may also be situations where Z_{DR} columns are not good indicators of updraft intensity especially when potential Z_{DR} columns are masked by three-body scatter spikes and/or the presence of large hail stones near the updraft (e.g., Kuster et al. 2019). Future work that considers a larger sample of cases from across the United States could address some of these questions and limitations.

Designing new VCPs, radar systems, and adaptive scanning capabilities for those radar systems that can increase vertical data coverage and decrease volumetric update time will likely lead to improved sampling of Z_{DR} columns and more effective use of the signature during warning operations. This idea includes forecast offices and forecasters determining which available scanning strategies are most effective at sampling the most important radar signatures for ongoing warning operations. It is probable that frequent low-level updates provided by techniques such as the supplemental adaptive intravolume low-level scans (SAILS; Crum et al. 2013) may not always be most effective especially when mid- and upper-level signatures, like Z_{DR} columns, provide crucial information for issuing warnings. In addition to faster update times, a future dual-pol phased array radar system may also allow for adaptive scanning capabilities (e.g., Heinselman and Torres 2011; Torres et al. 2014; Schvartzman et al. 2017; Torres et al. 2018). For example, different VCPs could be used in different sectors or for different storms based on storm type, range, etc. This capability could allow for VCPs to be used that would maximize vertical data coverage for storms at varying ranges without dramatically sacrificing update time or effective sampling of storms closer to the radar, thereby allowing forecasters to more efficiently observe Z_{DR} columns across a greater area within their county warning area.

Acknowledgments. CK thanks God for providing the opportunity and talented research team to accomplish this work. Specifically, the authors thank Jason Furtado for help with statistical analysis methods; Eddie Forren for KOUN data processing; Jeff Brogden, Robert Toomey, and Karen Cooper for help with WDSS-II; Danny Wasielewski, Micheal Shattuck, Allen Zahrai, and Rafael Mendoza for KOUN data collection support; and six NWS Norman Forecast Office employees (Ryan Barnes, Randy Bowers, Vivek Mahale, Doug Speheger, Richard Smith, and David Andra) for providing and enabling operational guidance on radar data analysis. We also thank Jami Boettcher, Randy Bowers, and Jacob Carlin for helpful reviews of this paper; Tanya Riley, Tracy Reinke, Jamie Foucher, and Colleen Hickman for help with administrative logistics; Steve Fletcher, Chris Carter, and everyone at NSSL IT for help with computer software/hardware issues; and Emma Kuster for support and helpful research discussions. We also thank the three anonymous reviewers who helped us greatly improve the quality of this article. Funding for CK and TS was provided by NOAA/Office of Oceanic and Atmospheric Research under NOAA–University of Oklahoma Cooperative Agreement NA16OAR4320115, U.S. Department of Commerce.

Data availability statement. All KOUN radar data used in this study are available by request from the National Severe Storms Laboratory.

REFERENCES

Andra, D. L., E. M. Quoetone, and W. F. Bunting, 2002: Warning decision-making: The relative roles of conceptual models, technology, strategy, and forecaster expertise on 3 May 1999. *Wea. Forecasting*, **17**, 559–566, https://doi.org/10.1175/1520-0434(2002)017<0559:WDMTRR>2.0.CO;2.

Bowden, K. A., P. L. Heinselman, D. M. Kingfield, and R. P. Thomas, 2015: Impacts of phased-array radar data on forecaster performance during severe hail and wind events. *Wea. Forecasting*, **30**, 389–404, https://doi.org/10.1175/WAF-D-14-00101.1.

Brotzge, J., and W. Donner, 2013: The tornado warning process: A review of current research, challenges, and opportunities. *Bull. Amer. Meteor. Soc.*, **94**, 1715–1733, https://doi.org/10.1175/BAMS-D-12-00147.1.

Browning, K. A., and R. J. Donaldson, 1963: Airflow and structure of a tornadic storm. *J. Atmos. Sci.*, **20**, 533–545, https://doi.org/10.1175/1520-0469(1963)020<0533:AASOAT>2.0.CO;2.

Crowe, C. C., C. J. Schultz, M. Kumjian, L. D. Carey, and W. A. Peterson, 2012: Use of dual-polarization signatures in diagnosing tornadic potential. *Electron. J. Oper. Meteor.*, **13**, 57–78.

Crum, T. D., S. D. Smith, J. N. Chrisman, R. E. Saffle, R. W. Hall, and R. J. Vogt, 2013: WSR-88D radar projects—Update 2013. *Proc. 29th Conf. on Environmental Information Processing Technologies*, Austin, TX, Amer. Meteor. Soc., 6B.1, https://ams.confex.com/ams/93Annual/webprogram/Paper221461.html.

Heinselman, P. L., and S. M. Torres, 2011: High-temporal-resolution capabilities of the National Weather Radar Testbed Phased-Array Radar. *J. Appl. Meteor. Climatol.*, **50**, 579–593, https://doi.org/10.1175/2010JAMC2588.1.

Herzegh, P. H., and A. R. Jameson, 1992: Observing precipitation through dual-polarization radar measurements. *Bull. Amer. Meteor. Soc.*, **73**, 1365–1374, https://doi.org/10.1175/1520-0477(1992)073<1365:OPTDPR>2.0.CO;2.

Illingworth, A. J., J. W. F. Goddard, and S. M. Cherry, 1987: Polarization radar studies of precipitation development in convective storms. *Quart. J. Roy. Meteor. Soc.*, **113**, 469–489, https://doi.org/10.1002/qj.49711347604.

Johns, R. H., and C. A. Doswell III, 1992: Severe local storms forecasting. *Wea. Forecasting*, **7**, 588–612, https://doi.org/10.1175/1520-0434(1992)007<0588:SLSF>2.0.CO;2.

Knight, C. A., 2006: Very early formation of big, liquid drops revealed by Z_{DR} in continental cumulus. *J. Atmos. Sci.*, **63**, 1939–1953, https://doi.org/10.1175/JAS3721.1.

Krauss, T. W., and J. D. Marwitz, 1984: Precipitation processes within an Alberta supercell hailstorm. *J. Atmos. Sci.*, **41**, 1025–1035, https://doi.org/10.1175/1520-0469(1984)041<1025:PPWAAS>2.0.CO;2.

Kumjian, M. R., 2013: Principles and applications of dual-polarization weather radar. Part II: Warm and cold season applications. *J. Oper. Meteor.*, **1**, 243–264, https://doi.org/10.15191/nwajom.2013.0120.

——, and A. V. Ryzhkov, 2008: Polarimetric signatures in supercell thunderstorms. *J. Appl. Meteor. Climatol.*, **47**, 1940–1961, https://doi.org/10.1175/2007JAMC1874.1.

——, A. P. Khain, N. Benmoshe, E. Ilotoviz, A. V. Ryzhkov, and V. T. J. Phillips, 2014: The anatomy and physics of Z_{DR} columns: Investigating a polarimetric radar signature with a spectral bin microphysical model. *J. Appl. Meteor. Climatol.*, **53**, 1820–1843, https://doi.org/10.1175/JAMC-D-13-0354.1.

Kuster, C. M., J. C. Snyder, T. J. Schuur, T. T. Lindley, P. L. Heinselman, J. C. Furtado, J. W. Brogden, and R. Toomey, 2019: Rapid-update radar observations of Z_{DR} column depth and its use in the warning decision process. *Wea. Forecasting*, **34**, 1173–1188, https://doi.org/10.1175/WAF-D-19-0024.1.

Lakshmanan, V., and A. Witt, 1997: A fuzzy logic approach to detecting severe updrafts. *AI Appl.*, **11**, 1–12.

——, T. Smith, G. J. Stumpf, and K. Hondl, 2007: The Warning Decision Support System-Integrated Information. *Wea. Forecasting*, **22**, 596–612, https://doi.org/10.1175/WAF1009.1.

Lemon, L. R., 1977: New severe thunderstorm radar identification techniques and warning criteria: A preliminary report. NOAA Tech. Memo. NWS NSSFC-1, 60 pp.

——, and C. A. Doswell III, 1979: Severe thunderstorm evolution and mesocyclone structure as related to tornadogenesis. *Mon. Wea. Rev.*, **107**, 1184–1197, https://doi.org/10.1175/1520-0493(1979)107<1184:STEAMS>2.0.CO;2.

Liu, X., K. Zhou, Y. Lan, X. Mao, and R. J. Trapp, 2020: On the construction principle of conceptual models for severe convective weather forecasting operations in China. *Wea. Forecasting*, **35**, 299–308, https://doi.org/10.1175/WAF-D-19-0026.1.

Moller, A. R., C. A. Doswell III, M. P. Foster, and G. R. Woodall, 1994: The operational recognition of supercell thunderstorm environments and storm structures. *Wea. Forecasting*, **9**, 327–347, https://doi.org/10.1175/1520-0434(1994)009<0327:TOROST>2.0.CO;2.

Nelson, S. P., 1983: The influence of storm inflow structure on hail growth. *J. Atmos. Sci.*, **40**, 1965–1983, https://doi.org/10.1175/1520-0469(1983)040<1965:TIOSFS>2.0.CO;2.

NOAA, 2013: Dual-polarization radar: Stepping stones to building a Weather-Ready Nation. NOAA, accessed 1 May 2018, https://www.weather.gov/news/130425-dualpol.

Picca, J. C., and A. V. Ryzhkov, 2012: A dual-wavelength polarimetric analysis of the 16 May 2010 Oklahoma City extreme hailstorm. *Mon. Wea. Rev.*, **140**, 1385–1403, https://doi.org/10.1175/MWR-D-11-00112.1.

——, M. R. Kumjian, and A. V. Ryzhkov, 2010: Z_{DR} columns as a predictive tool for hail growth and storm evaluation. *25th Conf. on Severe Local Storms*, Denver, CO, Amer. Meteor. Soc., 11.3, https://ams.confex.com/ams/25SLS/webprogram/Paper175750.html.

Romine, G. S., D. W. Burgess, and R. B. Wilhelmson, 2008: A dual-polarization-radar-based assessment of the 8 May 2003 Oklahoma City area tornadic supercell. *Mon. Wea. Rev.*, **136**, 2849–2870, https://doi.org/10.1175/2008MWR2330.1.

Ryzhkov, A. V., V. B. Zhuravlyov, and N. A. Rybakova, 1994: Preliminary results of X-band polarization radar studies of clouds and precipitation. *J. Atmos. Oceanic Technol.*, **11**, 132–139, https://doi.org/10.1175/1520-0426(1994)011<0132:PROXBP>2.0.CO;2.

Schvartzman, D., S. M. Torres, and Y. Tian-You, 2017: Weather radar spatiotemporal saliency: A first look at an information theory-based human attention model adapted to reflectivity images. *J. Atmos. Oceanic Technol.*, **34**, 137–152, https://doi.org/10.1175/JTECH-D-16-0092.1.

Snyder, J. C., A. V. Ryzhkov, M. R. Kumjian, A. P. Khain, and J. C. Picca, 2015: A Z_{DR} column detection algorithm to examine convective storm updrafts. *Wea. Forecasting*, **30**, 1819–1844, https://doi.org/10.1175/WAF-D-15-0068.1.

Torres, S. M., and Coauthors, 2014: A demonstration of adaptive weather surveillance and multifunction capabilities on the National Weather Radar Testbed Phased Array Radar. Preprints, *2014 Int. Radar Conf.*, Lille, France, IEEE, 1–6, https://doi.org/10.1109/RADAR.2014.7060420.

——, J. Boettcher, C. Curtis, F. Nai, and D. Schvartzman, 2018: Can an MPAR solution for SENSR meet all weather-surveillance mission-critical needs? Preprints, 2018 IEEE Radar Conf., Oklahoma City, OK, IEEE, 67–71, https://doi.org/10.1109/RADAR.2018.8378532.

Trapp, R. J., D. M. Wheatley, N. T. Atkins, R. W. Przybylinski, and R. Wolf, 2006: Buyer beware: Some words of caution on the use of severe wind reports in postevent assessment and research. *Wea. Forecasting*, **21**, 408–415, https://doi.org/10.1175/WAF925.1.

Tuttle, J. D., V. N. Bringi, H. D. Orville, and F. J. Kopp, 1989: Multiparameter radar study of a microburst: Comparison with model results. *J. Atmos. Sci.*, **46**, 601–620, https://doi.org/10.1175/1520-0469(1989)046<0601:MRSOAM>2.0.CO;2.

Van Den Broeke, M. S., 2017: Polarimetric radar metrics related to tornado life cycles and intensity in supercell storms. *Mon. Wea. Rev.*, **145**, 3671–3686, https://doi.org/10.1175/MWR-D-16-0453.1.

——, 2020: A preliminary polarimetric radar comparison of pretornadic and nontornadic supercell storms. *Mon. Wea. Rev.*, **148**, 1567–1584, https://doi.org/10.1175/MWR-D-19-0296.1.

Witt, A., M. D. Eilts, G. J. Stumpf, J. T. Johnson, E. D. Mitchell, and K. W. Thomas, 1998: An enhanced hail detection algorithm for the WSR-88D. *Wea. Forecasting*, **13**, 286–303, https://doi.org/10.1175/1520-0434(1998)013<0286:AEHDAF>2.0.CO;2.

Zrnić, D. S., and Coauthors, 2007: Agile-beam phased array radar for weather observations. *Bull. Amer. Meteor. Soc.*, **88**, 1753–1766, https://doi.org/10.1175/BAMS-88-11-1753.